Field-Extracted Lumped-Element Models of Coplanar Stripline Circuits and Discontinuities for Accurate Radio-Frequency Design and Optimization

Lei Zhu, *Senior Member, IEEE*, and Ke Wu, *Fellow, IEEE*

***Abstract*—In this paper, we present original lumped-element models of a large variety of coplanar stripline (CPS) circuits and discontinuities for accurate design and optimization of radio-frequency integrated circuits. These circuit models are extracted by applying a recently proposed deembedding technique called short-open calibration to calibrate the calculated field parameters obtained from the full-wave method of moments (MoM). It is realized by defining the two calibration standards, i.e., short and open elements, to evaluate and remove the error terms existing in the deterministic MoM algorithm, such as the approximation of port discontinuity and inconsistency of two-dimensional and three-dimensional characterizations of CPS external lines. In contrast to the static models, these field-extracted models can account for all the physical effects subject to the core area of CPS discontinuity, including frequency dispersion, high-order modes, and radiation loss. With this scheme, several CPS circuits and discontinuities are investigated over a wide frequency range to formulate their lumped-element models and also to expose their interesting features in connection with electrically finite width of the two strip conductors.**

***Index Terms*—Coplanar stripline discontinuity, lumped-element model, method of moments, short-open calibration technique.**

I. Introduction

COPLANAR stripline (CPS) [1] has recently gained a significant momentum in the design and applications of high-density radio-frequency integrated circuits (RFICs). The CPS geometry may be viewed as the dual structure of coplanar waveguide (CPW). With the arrangement of its two strips on a common dielectric interface, the CPS has all of the attractive features of its CPW counterpart, namely, easy insertion of shunt and series passive and active devices, and no need for via-holes to connect the ground plane [2]. In addition, the CPS presents some additional advantages over the CPW in that it eliminates the requirement of designing air-bridges around discontinuity to suppress the unwanted mode, as in the CPW [2]. The balanced geometry of the CPS offers flexibility in the design of uniplanar balanced circuits such as a uniplanar broad-band double-balanced mixer [3] and lumped-element CPS low-pass filter [4], as well as a CPS-fed printed dipole antenna array [5].

As compared to the extensive work on microstrip and CPW structures, few investigations have been carried out to date for studying electrical behavior of CPS discontinuities/elements and developing their computer-aided design (CAD) models that are useful for the design of passive and active CPS circuits and antennas. Very recently, a limited characterization of some simple CPS circuits [6]–[8] has been reported with resorting to a finite-difference time-domain (FDTD) method, as well as experimental procedures. Otherwise, a full-wave spectral-domain method was used for the characterization of a simple CPS open circuit [9], [10]. Still, it is desirable to formulate accurate equivalent lumped-element models of a large variety of CPS basic circuits and discontinuities for general-purpose design and optimization. Parasitic and dispersion effects should be rigorously accounted for in the models, which can be achieved only by a parameter extraction from some adequate field-based technique. This is important for a uniplanar CPS structure because its ground plane is always finite and it may generate intolerable parasitic effects, as will be shown in this paper. Specifically, additional series inductance and potential radiation caused by some CPS discontinuities in unbalanced CPS circuits, namely, CPS gap, may be quite severe, which cannot be ignored in the models.

In response to the above demands, a deterministic method of moments (MoM) algorithm, as detailed in [11], is extended for field modeling of the CPS structures. This is made possible by introducing an impressed electric field across the two strip conductors of CPS feed lines at the port planes of choice [12], [13]. Inspired from the concept of experimental calibration procedure [14], a numerical calibration technique, namely, short-open calibration (SOC) [15]–[17], was implemented to calibrate the MoM-based calculated parameters by removing the error terms existing in the 3-D MoM algorithm. These terms stand for the approximation of impressed fields at the ports and inconsistency of two-dimensional (2-D) and three-dimensional (3-D) characterizations of CPS external lines, when the deembedding procedure is required in the formulation of equivalent CAD model as to the preferable reference planes. With the proposed SOC

Manuscript received May 26, 1999; revised November 6, 2000. This work was supported by the Natural Sciences and Engineering Research Council of Canada.

L. Zhu is with the School of Electrical and Electronic Engineering, Nanyang Technological University, Singapore 639798 (e-mail: EZhuL@ntu.edu.sg).

K. Wu is with the Poly-Grames Research Center and Department of Electrical and Computer Engineering, Ecole Polytechnique de Montreal, Montreal, QC, Canada H3C 3A7 (e-mail: wuke@grmes.polymtl.ca).

Publisher Item Identifier S 0018-9480(02)03022-3.

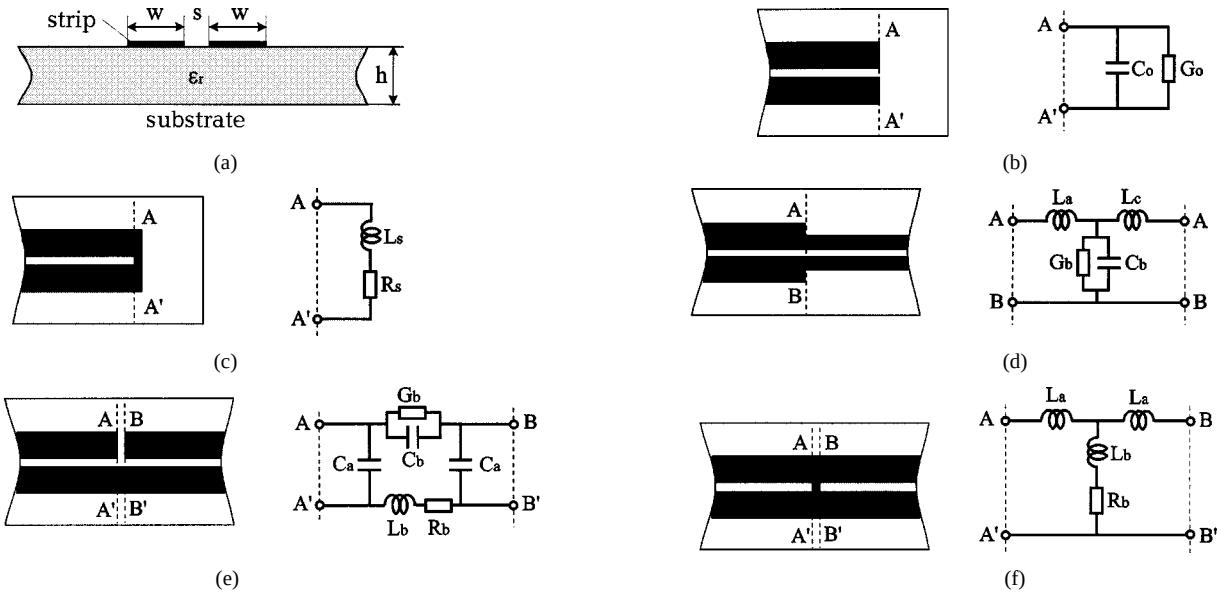

Fig. 1. Geometrical description, layout view, and equivalent-circuit model of CPS circuits and discontinuities. (a) Cross section of a uniform line. (b) Open circuit. (c) Short circuit. (d) Step discontinuity. (e) Capacitively coupled circuit (gap). (f) Inductively coupled circuit.

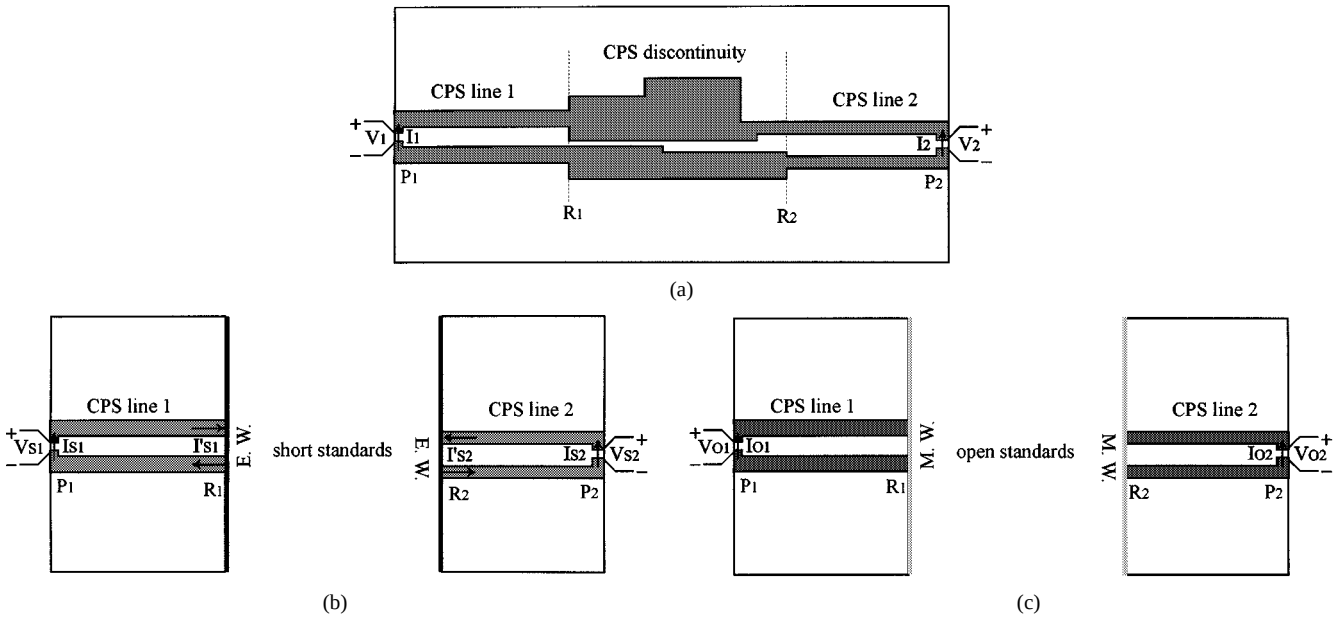

Fig. 2. Physical layout for the MoM characterization of a general CPS discontinuity and algorithmic arrangement of the two standard elements for the SOC parametric extraction of models from the MoM calculations. (a) Discontinuity layout. (b) Short standard element. (c) Open standard element.

technique, a very accurate equivalent-circuit model of a CPS circuit or discontinuity can be extracted from its physical layout, which accounts for all the physical effects such as frequency dispersion, high-order modes, and radiation loss. Interesting and unique features of CPS structures are described for the first time with their equivalent circuit. Comparison is also made with available data of some simple CPS circuits.

II. Field Modeling and Parametric Extraction of CPS Circuits

Fig. 1(a) describes a uniform CPS with its cross-sectional view, and the two strip conductors with identical width are printed on the top interface of a dielectric substrate. Fig. 1(b)–(f) show the top view of selected CPS discontinuities and their related lumped-element circuit models, namely, open, short, step, capacitively, and inductively coupled circuits. Note that it is not necessary to know *a priori* the equivalent lumped-element network since the SOC technique will extract the parameters in a self-consistent manner. In the following, a short narrative description will be given for the algorithm.

A. Deterministic MoM Algorithm

Fig. 2(a) gives the geometry of a generalized CPS discontinuity for the MoM characterization, which is externally connected with two different CPS lines. One of the difficulties in the development of a deterministic MoM algorithm is how to effectively represent the impressed fields along the external feed lines

having different widths, which is usually called "the excitation mechanism" [18]. To explicitly derive the circuit parameters from our MoM calculation, an impressed electric field is introduced between the two strip conductors of two individual CPS lines at adequate planes of reference. As in Fig. 2(a), the port topology is formulated by longitudinally truncating and transversely extending the two strip conductors. Of course, the port locations are chosen electrically far away from the CPS discontinuity such that the parasitic interaction among the fields of the ports and the discontinuity is avoided.

As described in [11], an electric-field integral equation (EFIE) governing the electric current density $(\vec{J})$ over the entire strip surface of the CPS lines and discontinuity can be derived in relation to the impressed electric field $(\vec{E}^{\rm im})$ at the port planes. Applying the Galerkin's technique leads to a source-type matrix equation, allowing the calculation of the unknown current density distributed at each port location and CPS lines, as well as the discontinuity. To involve a numerical calibration procedure in our MoM algorithm, the entire CPS circuit is further classified into two parts, separated by two additional reference planes (R_1 and R_2): two uniform line blocks in which propagates only a dominant mode excited by the voltage launcher, and discontinuity region to which all the discontinuity effects are attributed. This geometrical arrangement is inspired by the basic concept of the well-known experimental calibration procedure, e.g., [14], namely, error boxes and device-under-test (DUT).

B. SOC Calibration Scheme

The proposed SOC technique is then integrated with our MoM algorithm described above. It allows the parametric extraction of the core part of the CPS discontinuity (DUT) by evaluating and removing the two error boxes, which account for the port discontinuity and 3-D behavior of a uniform CPS line section for each external line. These error terms may bring about a "numerical noise" if a direct deembedding procedure is implemented that only relies on the 2-D behavior of a uniform CPS line section such as the characteristic impedance and electrical length. Even though very small, these terms are usually frequency or geometry dependent, as explained in [15]. Thus, they may be extremely harmful in the parameter extraction, considering that the CPS discontinuities of Fig. 1 are electrically small. This is because the lumped-element values of these discontinuities may become comparable with those of the error terms in this case.

The SOC technique requires two standard CPS short and open elements, as shown in Fig. 2(b) and (c), in connection with the two external lines of the CPS discontinuity. They are used to evaluate electrical behaviors of each CPS line section between the port location and the reference plane of the discontinuity, as depicted in Fig. 2(a). In the algorithm, the two standard elements can exactly be formulated by exciting a pair of odd and even impressed voltages at the two ports of a uniform CPS line with its length twice that of the corresponding CPS line section. In this way, the central location of the line can ideally be simulated by perfect electric (short-end) or magnetic (open-end) wall. Therefore, the uniform CPS line is divided into two identical parts, one of which represents the geometrical layout of the CPS short or open element. Via a 3-D MoM characterization of the two CPS elements, the current profile over the entire strip surface can be calculated. As the currents flowing at the port planes of the two CPS standard elements are derived, the error terms (boxes) between the ports and reference planes of the CPS discontinuity can analytically be formulated through the solution of three groups of equation on the basis of network theory. Further, the characteristic $ABCD$ matrix $[X_i]$ can be derived in a closed form by using the port currents upon the two excitations, and the current flowing at the short end, namely, I_{si}, I_{oi}, and I'_{si}, normalized with respect to the port voltages V_{si} and V_{oi} for the ith CPS external line

$$[X_i] = \begin{bmatrix} \dfrac{\bar{I}_{si}}{\bar{I}'_{si}} & -\dfrac{I}{\bar{I}'_{si}} \\ -\dfrac{\bar{I}'_{si}\bar{I}_{oi}}{\bar{I}_{si}-\bar{I}_{oi}} & \dfrac{\bar{I}'_{si}}{\bar{I}_{si}-\bar{I}_{oi}} \end{bmatrix} \tag{1}$$

in which, $\bar{I}_{si}$, $\bar{I}_{oi}$, and $\bar{I}'_{si}$ represent the three normalized currents. Thus, the error terms related to the CPS lines can accurately be evaluated and removed from the calculated results.

III. CPS Circuit Models and Discussion

With the proposed SOC scheme in the MoM algorithm, a CPS circuit or discontinuity layout can be characterized as a general-purpose equivalent-circuit model with accurately extracted lumped elements. We begin with the investigation on the numerical stability and accuracy of our SOC scheme in the 3-D MoM by modeling of a simple CPS open circuit, prior to dealing with a variety of CPS circuits and discontinuities. Our special interests in this study are focused on the theoretical study of parasitic effects happening around the discontinuity of unbalanced CPS circuits, which are essentially generated by the finite strip width of the CPS lines.

A. Open Circuit

Let us look at the circuit model and electrical characteristics of a CPS open circuit, as depicted in Fig. 1(b). Strictly speaking, the open end should equivalently be modeled as a shunt capacitance C_0 and conductance G_0, standing for the fringing and radiating effects. These circuit parameters have been studied to some extent with a quasi-TEM model [19], thru-reflection line (TRL) measurements, and FDTD [6] as well as spectral-domain methods [9]. Unfortunately, there exist some intolerable differences among them and also strong frequency-dependent (or distributed) characteristics of all the deembedded shunt capacitance C_0. To our knowledge, it is basically attributed to the fact in the deembedding procedures that all the parasitic effects at the incident or input port in the numerical technique [6], [9] are completely ignored while the short-end element defined in the TRL measurements [6] is not a perfect reflection standard. Following the description in [11], they are very harmful in the parametric extraction of an electrically small CPS open circuit in such a way that the extracted C_0 strongly depends on the operating frequency and external line length of choice. To validate the effectiveness of any deembedding procedure, one of

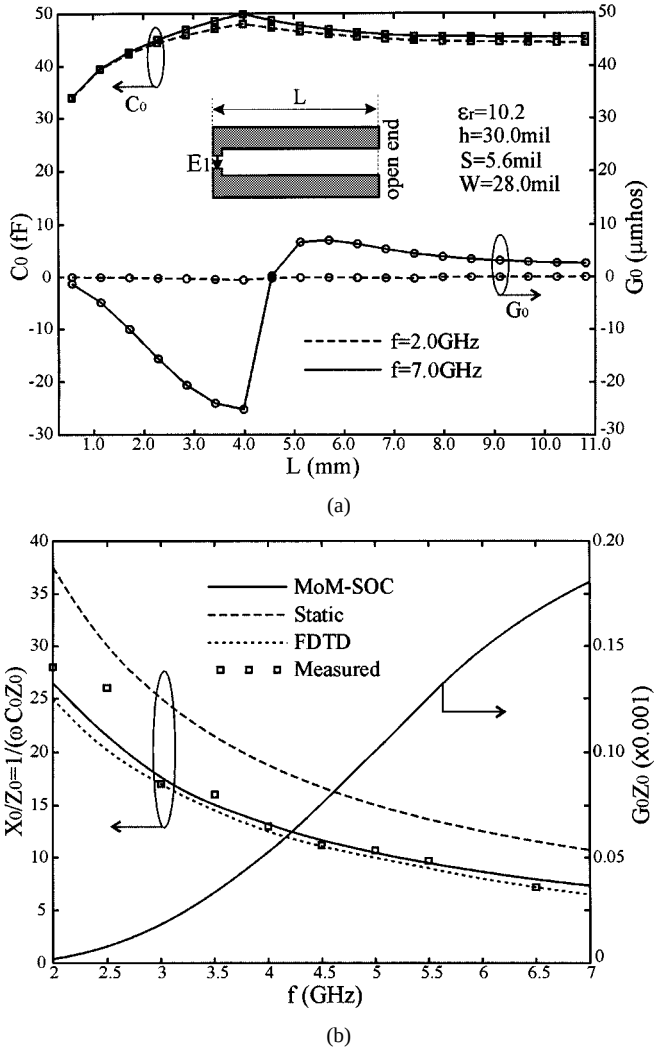

Fig. 3. Extracted complex admittance ($Y_o = G_o + jB_o$) of a CPS open circuit. (a) Numerical convergence versus the feed-line length (L). (b) Comparison with other theoretical and experimental results.

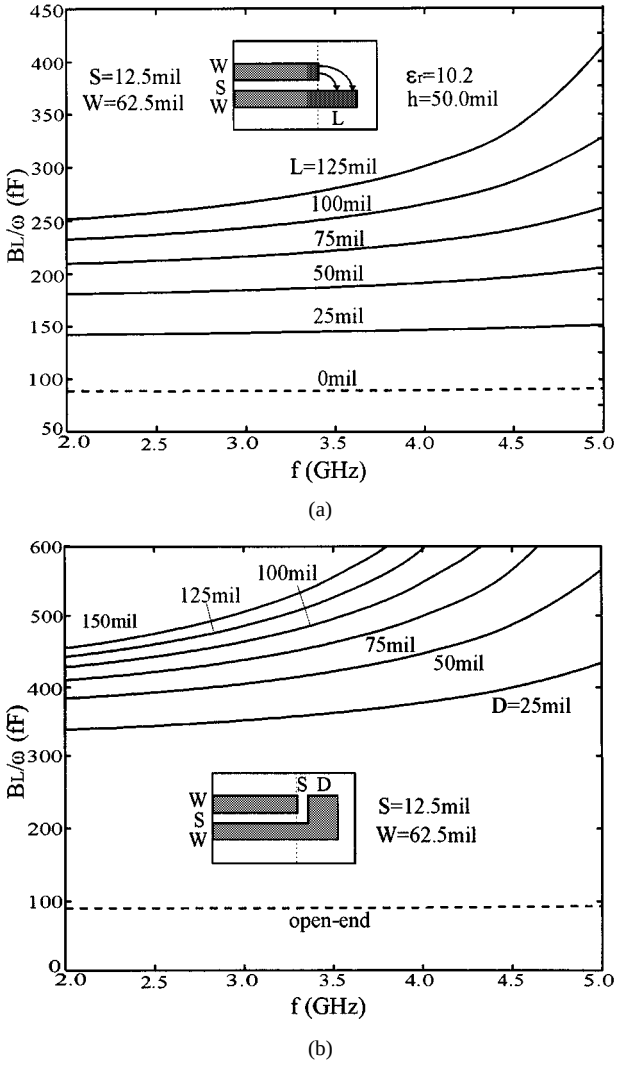

Fig. 4. Parametric behavior of the extracted susceptance for two nonstandard CPS open circuits with extended line (called "type-A") and bent-line 90° section (called "type-B") as a function of frequency. (a) Type-A. (b) Type-B.

the standard procedures is to check whether the extracted circuit parameters are independent of the different external CPS lines (L).

Fig. 3(a) depicts our extracted capacitance (C_0) and conductance (G_0) of a simple CPS open circuit against the CPS feed-line length (L) at frequencies $f = 2.0$ *and* 7.0 GHz. For the length (L) shorter than 7.0 mm, both C_0 and G_0 appears significantly related to L, especially for G_0 in the case of $f = 7.0$ GHz. It may be attributed to a parasitic interaction of fields at the open-end and the port location over this short line range. As L is extended beyond 7.0 mm, they gradually converge to some stable values, representing their relative lumped-element parameters at the two specific frequencies. This result indicates that the problem of length-dependent instability can completely be solved with our SOC scheme if the port location is chosen far away from the core discontinuity.

Fig. 3(b) gives a general comparison of our extracted parameters against the other results over the frequency range of interest for the normalized reactance X_0/Z_0, as in [6]. Our X_0/Z_0 is much closer to the FDTD results than the static and measured results over the frequency range from 2.0 to 7.0 GHz. Further, the extracted C_0 is found well stationary at the value of 44.8 fF within a variation of 1.5%, thus exhibiting the lumped-element behavior of the CPS open circuit. The extracted G_0 shows an exponential increase and then a linear increment with f, but its value is extremely smaller, as compared to its real counterpart B_0 or $1/X_0$.

As compared with the infinitely extended ground plane of the other planar lines such as microstrip and CPW, the two strip widths of a CPS line are electrically narrow, susceptibly giving rise to a nonnegligible influence on electrical behaviors of some CPS circuits. In [6], a CPS circuit with an extended strip conductor was modeled as a lumped capacitance and it was found to be equal to three or four times of its conventional counterpart for a selected dimension. However, no detailed discussion was given as to its operating principle and physical insight. Judging from our extracted lumped elements of an open circuit (called "type-A") defined at its reference plane (open terminal), as shown in Fig. 4(a), we observe that the normalized susceptance B_L/ω exhibits an unexpectedly nonlinear behavior with frequency. This is much more pronounced with a large value of B_L/ω at higher frequency if one of the conductor strips is ex-

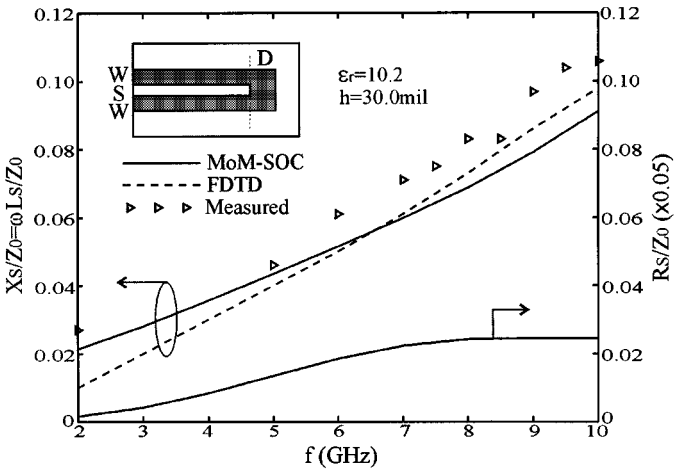

(a)

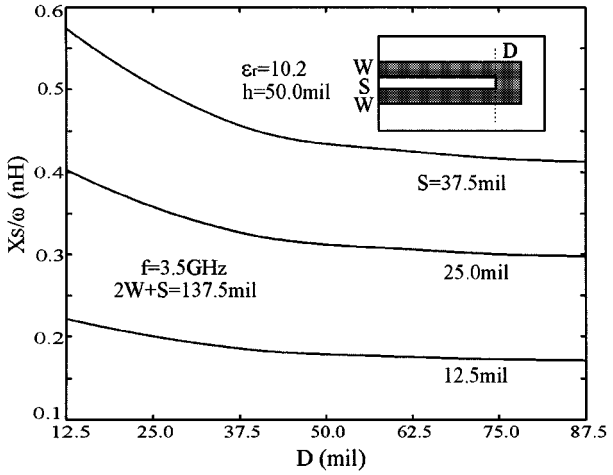

(b)

Fig. 5. Extracted complex short-end impedance $(Z_s = R_s + jX_s)$ of a CPS short circuit. (a) Comparison with the FDTD and experimental results. (b) Reactance (X_s/ω) versus the width (D).

tended largely beyond the other with a length of L. Quite similarly, such a nonlinear property of dispersion can also be found in the extracted model of the other CPS open circuit (called "type-B"), as indicated in Fig. 4(b), in which one of the strip conductors is bent around the other. This interesting phenomenon can be explained based on a distributed coupling theory. In fact, a fringing-field coupling takes place between the open end of the short line and the extended line. It can be expected that this coupling is frequency dependent. In this case, the coupled section can equivalently be described by a circuit model in terms of a group of distributed shunt capacitances and series inductances rather than a purely lumped-capacitance model, as in Fig. 1(b). In general, these series inductances are caused from the extended conductor section having a finite strip width.

B. Short Circuit

A CPS short circuit is realized by simply interconnecting the ends of two strip conductors, which can be described by a circuit model in terms of a series-connected inductance (L_S) and resistance (R_S), as shown in Fig. 1(c). Fig. 5(a) displays our extracted normalized reactance (X_S/Z_0) and resistance (R_S/Z_0) as a function of frequency against the FDTD and experimental

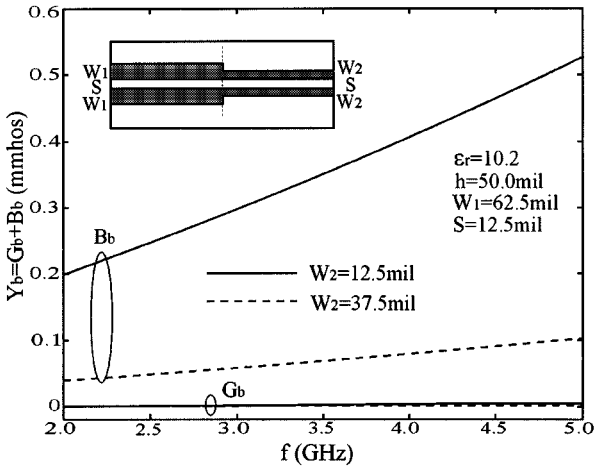

Fig. 6. Frequency-dependent shunt admittance $(Y_b = G_b + jB_b)$ of a CPS step discontinuity that is formed by two interconnecting strip widths (W_1 and W_2).

results [6]. Our X_S/Z_0 increases in an approximately linear function with frequency and agrees reasonably with the other results over a wide frequency range (2.0–10.0 GHz). Otherwise, R_S/Z_0 gradually rises up with frequency, representing the radiation loss from the transverse strip conductor with the width (D) at the CPS short-end. Fig. 5(b) shows the extracted X_S/Z_0 as a function of the strip width (D) at $f = 3.5$ GHz. It is found that X_S/Z_0 starts to increase and becomes more pronounced for a wide slot width (S) once the width (D) is chosen smaller than 50.0 mil. To form a better CPS short circuit, a preferred way is to choose the width (D) as wide as possible in reducing such an inductive effect of the short end. However, such a CPS short circuit definitely represents a nonnegligible inductance at the short end due to the finitely extended slot width (S) so that this circuit element cannot be perceived as a perfect reflection standard in the deembedding or calibration procedure [6].

C. Step Discontinuity

Similar to other planar structures, a CPS step discontinuity stands for an abruptly longitudinal change in linewidth, as described in Fig. 1(d), and its circuit model is generally represented with four lumped elements. In our calculations, only the complex shunt admittance $(Y_b = G_b + jB_b)$ is found to play a principal role in the entire equivalent network of such a CPS discontinuity. Fig. 6 gives our extracted shunt susceptance B_b and conductance G_b as a function of frequency for a CPS step discontinuity with a fixed slot width (S). In this case, B_b goes up as a good linear function of frequency, thus exhibiting an excellent lumped-capacitance characteristic. Also, it shifts up rapidly with the ratio of two different strip widths of this CPS step, e.g., W_1/W_2. On the other hand, G_b is found to increase visibly with frequency and width ratio (W_1/W_2), but it still seems negligibly small as compared to B_b over the frequency range.

D. Inductively Coupled Circuit

Fig. 1(f) describes a physical layout and its equivalent T-type circuit model of an inductively coupled CPS circuit with a transverse strip conductor bridging the two strip conductors. The equivalent network consists of four lumped-parameters, namely,

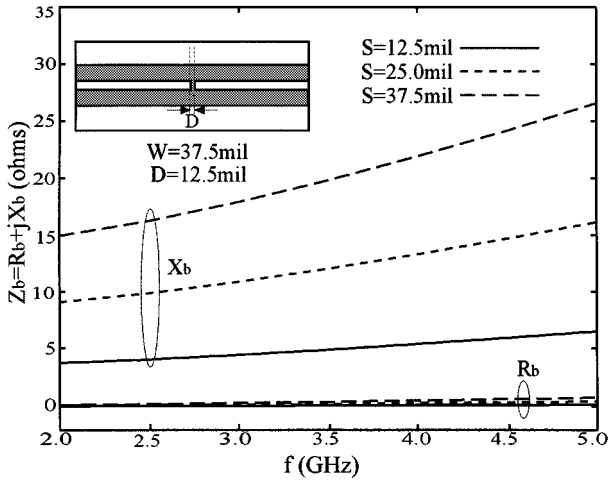

Fig. 7. Frequency-dependent shunt impedance $(Z_b = R_b + jX_b)$ of a CPS inductively coupled circuit with different CPW slot width (S).

self-resistance/mutual resistance and reactances R_a, R_b, X_a, and X_b. These parameters can effectively be extracted from the full-wave MoM via our SOC scheme. Fig. 7 depicts the extracted mutual R_b and X_b as a function of frequency versus different slot width (S) for a fixed narrow width $(D = 12.5\,\text{mil})$. It can be observed that X_b gradually increases with frequency (f) and rapidly shifts up as the slot width (S) is widened from 12.5 to 37.5 mil, exhibiting a great enhancement of its quasi-lumped series inductance (L_b). In parallel, R_b slightly rises up as f increases and S is widened, but it is smaller than X_b. On the other hand, R_a and X_a is also much small in the case of the narrow D and wide S so that this CPS circuit can well be modeled by a single shunt reactance X_b.

E. Capacitively Coupled Circuit

As our last example, a capacitively coupled circuit presents some interesting and distinct features of the CPS circuits. This circuit consists of an air gap along one of the strip conductors while the other line is kept intact and this structure was also called a "CPS series gap," as in [6]. Fig. 8(a) shows its geometrical view with a gap interval D. In [6], this structure was modeled as a lumped-capacitance π-network, and its FDTD-calculated parameters were plotted against measured ones at low frequency. Strictly speaking, its generalized circuit model should be considered as in Fig. 8(b) by adding a series inductance because the strip conductors have inherently electrically finite widths. This nonignorable parameter represents the parasitic effect of a noninfinitely extended strip width around the air gap section. The resulting circuit model of Fig. 8(b) can be converted into a π-network, as shown in Fig. 8(c), in which the series capacitance and inductance are put together to make up an equivalent series resonant circuit. In our MoM algorithm, any potential radiation loss [11]–[13] can be taken into account and can equivalently be incorporated into the model by a shunt conductance and a series resistance, as indicated in Fig. 8(b) and (c).

Fig. 9 shows our extracted circuit parameters over a wide frequency range (2.0–10.0 GHz) with the same dimensions as those in [6]. From Fig. 9(a), the self-susceptance (B_p) is found

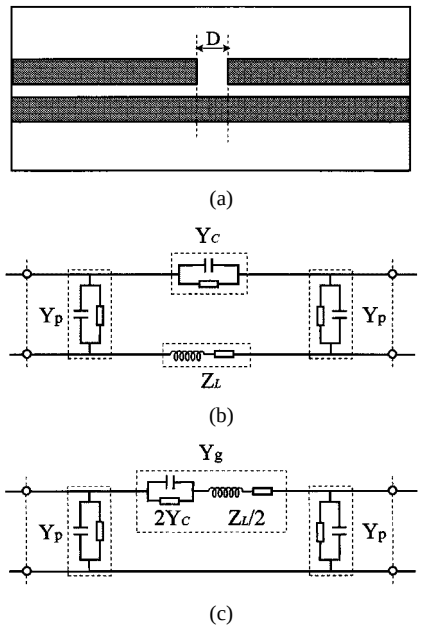

Fig. 8. Geometrical description and its possible equivalent circuit models of a CPS capacitively coupled (gap) circuit. (a) Top-view layout. (b) Original circuit model. (c) Convenient circuit model.

to linearly increase with frequency, while the self-conductance (G_p) appears unchanged and much smaller than B_p. Fig. 9(b) gives the frequency response of the mutual-conductance (G_g) and the mutual-susceptance (B_g), depicting a vivid behavior of some unexpected radiating resonance, which is caused by the simultaneous existence of a series gap capacitance and a series inductance. Usually, the capacitance is intuitively obtainable by static or full-wave solutions, whereas the inductance due to the grounding line or the line of reference may easily be overlooked in the modeling. Generally speaking, a large gap interval triggers a large inductance under the fixed W and S, such that the resonant frequency is significantly reduced because the capacitance (C) remains unchanged. Of course, the maximum radiation takes place around the frequency of resonance, translating the maximum value of G_g.

To validate our claimed results here, Fig. 10 gives a general comparison between our predicted results and those of [6], which depicts a frequency response of S-parameter characteristics for a structure with a wide strip width. Note that only low-frequency results are available in [6]. From our obtained curves, we can observe that a sharp variation of the S-parameters within the high portion of the frequency band is observed, which was not reported in [6]. This corresponds to a circuit resonance around $f = 7.4$ GHz, caused by a series gap capacitance and a series line inductance shown in Fig. 8(b) and (c). Interestingly, our recent work [20] demonstrates from both theory and experiments that such a resonant phenomenon exists in a finite-ground CPW gap circuit that also has an electrically finite-ground width. To our knowledge, there is a common physical mechanism for them that the finite ground at the same location as the gap interval (D) generates an additional series inductance in the complete model, as illustrated in Fig. 8(b).

Now, let us take a close look at some visible and nonnegligible difference among three sets of the independent results in

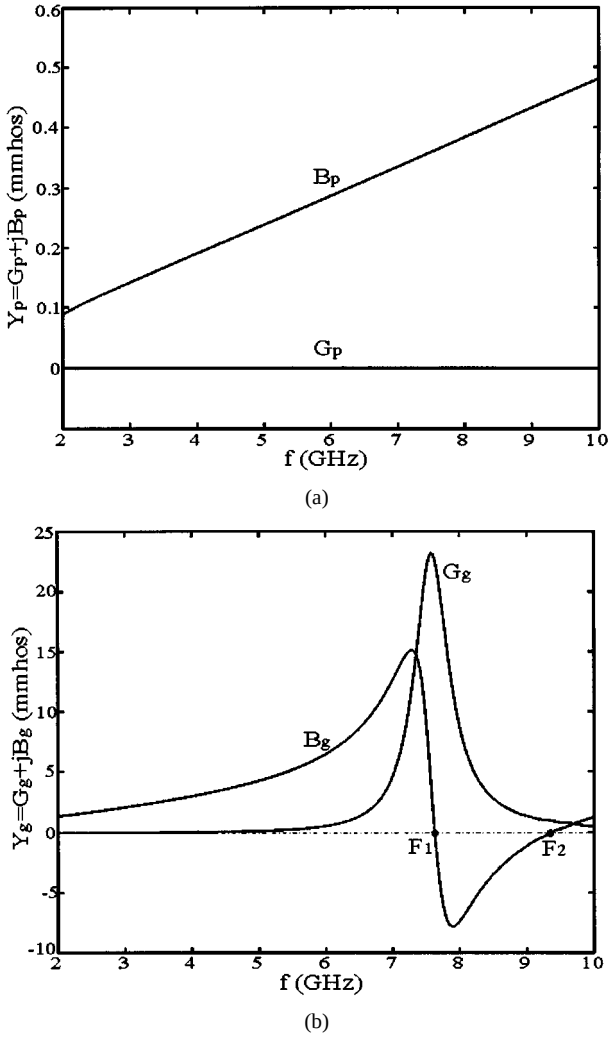

Fig. 9. Extracted complete circuit parameters of the CPS inductively coupled circuit. (a) Complex self-admittance ($Y_p = G_p + jB_p$). (b) Complex mutual-admittance ($Y_g = G_g + jB_g$).

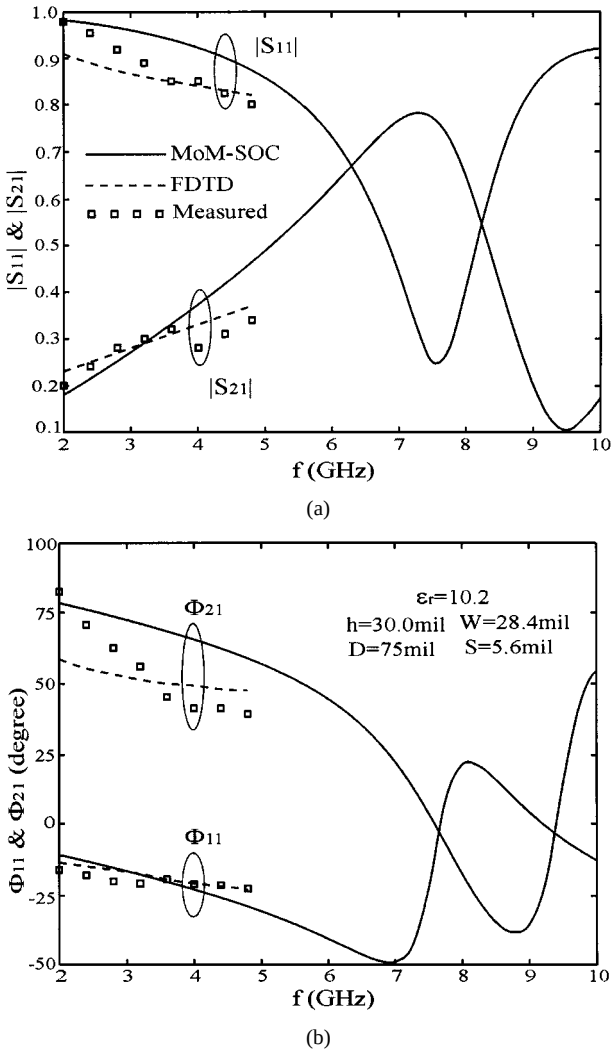

Fig. 10. Comparison of our calculated S-parameters against the FDTD and experimental results for a CPS capacitively coupled (gap) circuit, for which our results show an unexpected resonance around 7.6 GHz. (a) Magnitude of S-parameters: $|S_{11}|$ & $|S_{21}|$. (b) Phase of S-parameters: Φ_{11} & Φ_{21}.

both magnitudes ($|S_{11}|$ & $|S_{21}|$) and phases (Φ_{11} & Φ_{21}) of S-parameters, as illustrated in Fig. 10. According to the principle of a reciprocal, lossless, and symmetrical two-port network [21], these magnitude and phase parameters should rigorously be satisfied with the following two basic equations, i.e., $|S_{11}|^2+|S_{21}|^2 = 1$ and $(\Phi_{11}-\Phi_{21}) = (2n-1)90°$, where n is an integer number. Fig. 11 indicates the three sets of frequency-dependent loss factor $\left(1-|S_{11}|^2-|S_{21}|^2\right)$ and phase factor $(\Phi_{11}-\Phi_{21})$, which are directly obtained from the FDTD and experimental results, as well as our SOC results as in Fig. 10. Over the frequency range $(f < 4.8\,\text{GHz})$ regarding the case of an extremely low loss [6], our results show that the loss factor is lower than 0.02, while the phase factor is almost kept around 90°, exhibiting an excellent consistency with the condition of a lossless two-port network. Unfortunately, the FDTD and experimental results illustrate a high loss factor with some irregularly frequency dependency even at low frequency. On the other hand, the phase factor for the FDTD results is almost kept around 75° far away from 90° in the lossless case, while randomly changes between 60° and 100° for the measured ones. To our understanding, it is mainly attributed to the unsolved issues such as nonideal calibration standards in the measurement and the complete ignorance of the incident port discontinuity in the FDTD modeling for the parametric extraction of electrically small CPS circuits by using the existing deembedding procedures.

Furthermore, Fig. 11(a) illustrates a detailed radiation behavior of such a CPS gap discontinuity over a wide frequency range, in which the maximum radiation is observed to happen around the resonance with reference to Fig. 9(b). Fig. 11(b) indicates that the phase factor gradually goes down from the 90° line, drops off toward a negative minimum degree at a frequency location marked by "F_1," and then rises up to a positive degree as frequency is further increased beyond the location "F_2." With reference to the results in Fig. 9(b), we can further observe that the susceptance (B_g) is exactly equal to zero value at these two frequencies (F_1 and F_2) and becomes positive or negative values before or beyond them due to the capacitive or inductive B_g. Otherwise, we can observe that the phase factor is continuously varied as a function of frequency without any abrupt change, as in the lossless case regarding the dotted line in Fig. 11(b), and also its value is far away from the $\pm 90°$ lines, especially around the resonance. It can be well understood by the increasing radiation loss around the resonance, as shown in Fig. 9(b).

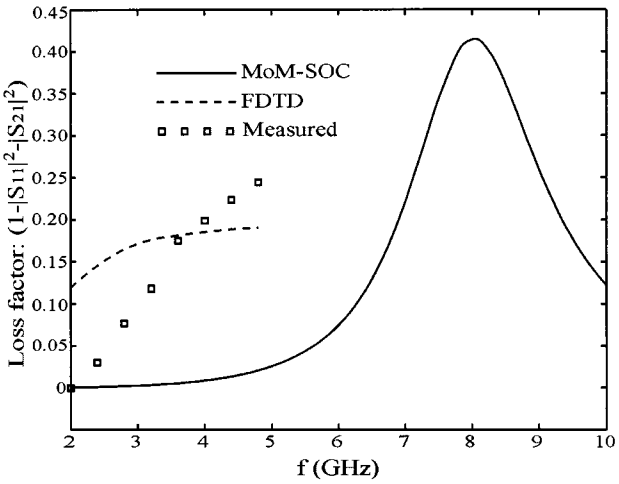

(a)

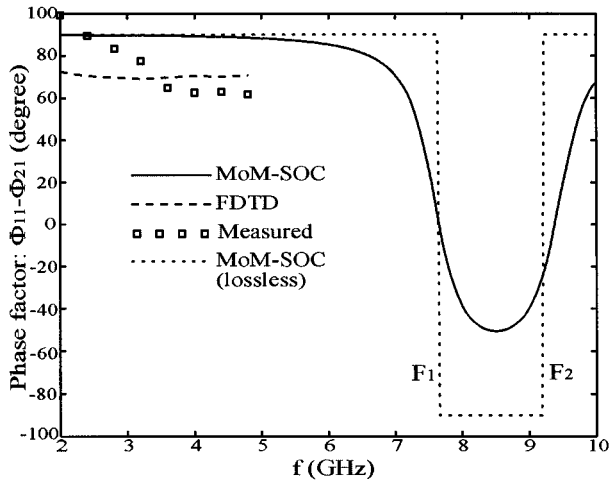

(b)

Fig. 11. Physical view of the three sets of S-parameters in Fig. 10 according to the principle of a reciprocal two-port network. (a) Loss factor: $(1-|S_{11}|^2-|S_{21}|^2)$. (b) Phase factor: $(\Phi_{11}-\Phi_{21})$ (in degrees).

IV. Conclusion

In this paper, a variety of uniplanar CPS circuits and discontinuities have been studied in depth with the use of a deterministic 3-D MoM algorithm that incorporates a numerical deembedding technique called SOC. This unique scheme allows one to remove (calibrate) potential errors of the algorithm and extract the core circuit parameters in a very accurate manner. Thus, equivalent lumped-element circuit models can be obtained from physical layouts of the CPS discontinuities without resorting to a pre-knowledge or presetting of their circuit behavior. Interesting and distinct features of the CPS discontinuities and circuits are presented with detailed results of the extracted circuit models. It is discussed and explained for the first time that the finite-ground line of unbalanced CPS structures may generate nonnegligible and significant parasitic effects including an unexpected inductance effect or potential radiation loss or parasitic resonance phenomenon. Our CAD-oriented models provide a robust physical understanding and some insightful design rules of this new transmission-line-based circuits and structures, which is emerging as one of the new-generation building blocks of high-density radio-frequency design.

Acknowledgment

The authors gratefully acknowledge the anonymous reviewers for their valuable comments, which enabled the authors to produce a more accurate and readable revised manuscript.

References

[1] J. B. Knorr and K. D. Kuchler, "Analysis of coupled slots and coplanar strips on dielectric substrate," *IEEE Trans. Microwave Theory Tech.*, vol. MTT-23, pp. 541–548, July 1975.

[2] K. C. Gupta, R. Garg, I. Bahl, and P. Bhartia, "Coplanar lines: Coplanar waveguide and coplanar strip," in *Microstrip Lines and Slotlines*, 2nd ed. Norwood, MA: Artech House, 1996, ch. VII.

[3] H. K. Chiou, C. Y. Chang, and H. H. Lin, "Balun design for uniplanar broadband double balanced mixer," *Electron. Lett.*, vol. 31, no. 24, pp. 2113–2114, 1995.

[4] S. G. Mao, H. K. Chiou, and C. H. Chen, "Modeling of lumped-element coplanar-stripline low-pass filter," *IEEE Microwave Guided Wave Lett.*, vol. 8, pp. 141–143, Mar. 1998.

[5] A. Nesic, V. Trifunovic, and B. Jokanovic, "Highly efficient two-dimensional printed antenna array with a new feeding network," in *Proc. 12th Eur. Microwave Conf.*, 1984, pp. 697–701.

[6] R. N. Simons, N. I. Dib, and L. P. B. Katehi, "Modeling of coplanar stripline discontinuities," *IEEE Trans. Microwave Theory Tech*, vol. 44, pp. 711–716, May 1996.

[7] K. Goverdhanam, R. N. Simons, and L. P. B. Katehi, "Coplanar stripline components for high-frequency applications," *IEEE Trans. Microwave Theory Tech*, vol. 45, pp. 1725–1729, Oct. 1997.

[8] ——, "Coplanar stripline propagation characteristics and bandpass filter," *IEEE Microwave Guided Wave Lett.*, vol. 7, pp. 214–216, Aug. 1997.

[9] H. Y. Wang, D. Mirshekar-Syahkal, and I. J. Dilworth, "Spectral domain analysis of coplanar strip discontinuities," *Microwave Opt. Technol. Lett.*, vol. 15, pp. 395–398, Aug. 1997.

[10] J. S. McLean, A. D. Wieck, K. Ploog, and T. Itoh, "Full-wave analysis of open-end discontinuities in coplanar stripline and finite ground plane coplanar waveguide in open environments using a deterministic spectral domain approach," in *Proc. 21st Eur. Microwave Conf.*, vol. 2, Sept. 1991, pp. 1004–1007.

[11] L. Zhu and K. Wu, "Characterization of unbounded multiport microstrip passive circuits using an explicit network-based method of moments," *IEEE Trans. Microwave Theory Tech*, pt. I, vol. 45, pp. 2114–2124, Dec. 1997.

[12] ——, "Circuit model and input impedance of feeding structures for coplanar stripline (CPS) printed dipole antenna," in *Proc. Asia–Pacific Microwave Conf.*, Dec. 1998, pp. 1397–1400.

[13] ——, "Model-based characterization of CPS-fed printed dipole for innovative design of uniplanar integrated antenna," *IEEE Microwave Guided Wave Lett.*, vol. 9, pp. 342–344, Sept. 1999.

[14] R. A. Soares, P. Gouzien, P. Legaud, and G. Follot, "A unified mathematical approach to two-port calibration techniques and some applications," *IEEE Trans. Microwave Theory Tech.*, vol. 37, pp. 1669–1674, Nov. 1989.

[15] L. Zhu and K. Wu, "Unified equivalent circuit model of planar discontinuities suitable for field theory-based CAD and optimization of M(H)MIC's," *IEEE Trans. Microwave Theory Tech.*, pt. I, vol. 47, pp. 1589–1602, Sept. 1999.

[16] ——, "Revisiting characteristic impedance and its definition of microstrip line with a self-calibration 3-D MoM scheme," *IEEE Microwave Guided Wave Lett.*, vol. 8, pp. 87–89, Feb. 1998.

[17] J. Ratio, "Comments on 'Revisiting characteristic impedance and its definition of microstrip line with a self-calibration 3-D MoM scheme'," *IEEE Trans. Microwave Theory Tech.*, vol. 47, pp. 115–119, Jan. 1999.

[18] T. S. Horng, N. G. Alexopoulos, S. C. Wu, and H. Y. Yang, "Full-wave spectral-domain analysis for open microstrip discontinuities of arbitrary shape including radiation and surface-wave losses," *Int. J. Microwave Millimeter-Wave Computer-Aided Eng.*, vol. 2, no. 4, pp. 224–240, 1992.

[19] W. J. Gesinger, "End-effects in quasi-TEM transmission lines," *IEEE Trans. Microwave Theory Tech.*, vol. 41, pp. 666–672, Apr. 1993.

[20] L. Zhu and K. Wu, "Unified CAD-oriented circuit model of finite-ground coplanar waveguide gap structure for uniplanar M(H)MIC's," in *IEEE MTT-S Int. Microwave Symp. Dig.*, Anaheim, CA, June 12–19, 1999, pp. 39–42.

[21] R. E. Collin, *Foundations for Microwave Engineering*, 2nd ed. New York: McGraw-Hill, 1992, pp. 254–257.

Lei Zhu (S'91–M'93–SM'00) was born in Wuxi, Jiangsu Province, China, in June 1963. He received the B.Eng. and M.Eng. degrees in radio engineering from the Nanjing Institute of Technology (now Southeast University), Nanjing, China, in 1985 and 1988, respectively, and the Ph.D. Eng. degree in electronic engineering from the University of Electro-Communications, Tokyo, Japan, in 1993.

From 1985 to 1989, he studied a variety of millimeter-wave passive and active circuits, and leaky-wave antennas using the grooved nonradiative dielectric waveguide (GNRD). From 1989 to 1993, he conducted research on the full-wave characterization and optimization design of planar integrated transmission lines and components. From 1993 to 1996, he was a Research Engineer with Matsushita-Kotobuki Electronics Industries Ltd., Tokyo, Japan, where he undertook research and development in the development of planar integrated antenna elements and arrays with compact-size and high radiation gain/efficiency for application in wireless communications. From 1996 to 2000, he was a Research Fellow with Ecole Polytechnique de Montreal, Montreal, QC, Canada. Since July 2000, he has been an Associate Professor with the School of Electrical and Electronic Engineering, Nanyang Technological University, Singapore. His current research works/interests include the study of planar integrated dual-mode filters, ultra-broad bandpass filters, broad-band interconnects, planar antenna elements/arrays, uniplanar CPW/CPS circuits, as well as full-wave 3-D MoM modeling of planar integrated circuits and antennas, numerical deembedding or parameter-extraction techniques, and field-theory-based CAD synthesis/optimization design procedures.

Dr. Zhu was the recipient of the Japanese Government (Monbusho) Graduate Fellowship (1989–1993). He was also the recipient of the 1993 First-Order Achievement Award in Science and Technology presented by the National Education Committee, China, the 1996 Silver Award of Excellent Invention presented by the Matsushita-Kotobuki Electronics Industries Ltd., Japan, and the 1997 Asia–Pacific Microwave Prize Award presented at the Asia–Pacific Microwave Conference, Hong Kong.

Ke Wu (M'87–SM'92–F'01) was born in Liyang, Jiangsu Province, China. He received the B.Sc. degree in radio engineering (with distinction) from the Nanjing Institute of Technology (now Southeast University), Nanjing, China, in 1982, and the D.E.A. and Ph.D. degrees in optics, optoelectronics, and microwave engineering (with distinction) from the Institut National Polytechnique de Grenoble (INPG), Grenoble, France, in 1984 and 1987, respectively.

He conducted research in the Laboratoire d'Electromagnetisme, Microondes et Optoelectronics (LEMO), Grenoble, France, prior to joining the Department of Electrical and Computer Engineering, University of Victoria, Victoria, BC, Canada. He subsequently joined the Department of Electrical and Computer Engineering, Ecole Polytechnique de Montreal (Faculty of Engineering, University of Montreal) as an Assistant Professor, and is currently a Full Professor and Canada Research Chair in Radio-Frequency and Millimeter-Wave Engineering. He has been a Visiting or Guest Professor at Telecom-Paris, Paris, France, and INP-Grenoble, Grenoble, France, the City University of Hong Kong, the Swiss Federal Institute of Technology (ETH-Zurich), Zurich, Switzerland, the National University of Singapore, Singapore, the University of Ulm, Ulm, Germany, as well as many short-term visiting professorships in other universities. He also holds an honorary visiting professorship at the Southeast University, Nanjing, China. He has been the Head of the FCAR Research Group of Quebec on RF and microwave electronics, and the Director of the Poly-Grames Research Center, as well as the Founding Director of the newly developed Canadian Facility for Advanced Millimeter-Wave Engineering (FAME). He has authored or co-authored over 300 referred journal and conference papers, and also several book chapters. His current research interests involve 3-D hybrid/monolithic planar and nonplanar integration techniques, active and passive circuits, antenna arrays, advanced field-theory-based CAD and modeling techniques, and development of low-cost RF and millimeter-wave transceivers. He is also interested in the modeling and design of microwave photonic circuits and systems. He serves on the Editorial Board of *Microwave and Optical Technology Letters*.

Dr. Wu is a member of Electromagnetics Academy. He was chairperson of the 1996 ANTEM Publicity Committee and vice-chairperson of the Technical Program Committee (TPC) for the 1997 Asia–Pacific Microwave Conference (APMC'97). He has served on the FCAR Grant Selection Committee and the TPC committee for the TELSIKS and ISRAMT. He has also served on the ISRAMT International Advisory Committee. He was the general co-chair of the 1999 and 2000 SPIE International Symposium on Terahertz and Gigahertz Electronics and Photonics, held in Denver, CO, and San Diego, CA, respectively. He was the general chair of 8th International Microwave and Optical Technology (ISMOT'2001), Montreal, QC, Canada, June 19–23, 2001. He has served on the Editorial or Review Boards of various technical journals, including the IEEE TRANSACTIONS ON MICROWAVE THEORY AND TECHNIQUES, the IEEE TRANSACTIONS ON ANTENNAS AND PROPAGATION, and the IEEE MICROWAVE AND GUIDED WAVE LETTERS. He served on the 1996 IEEE Admission and Advancement (A&A) Committee, the Steering Committee for the 1997 joint IEEE Antennas and Propagation Society (IEEE AP-S)/URSI International Symposium. He has also served as a TPC member for the IEEE Microwave Theory and Techniques Society (IEEE MTT-S) International Microwave Symposium. He was elected into the Board of Directors of the Canadian Institute for Telecommunication Research (CITR). He serves on the Technical Advisory Board of Lumenon Lightwave Technology Inc. He is currently the chair of the joint IEEE chapters of MTT-S/AP-S/LEOS in Montreal, QC, Canada. He was the recipient of a URSI Young Scientist Award, the Institute of Electrical Engineers (IEE), U.K., Oliver Lodge Premium Award, the Asia–Pacific Microwave Prize Award, the University Research Award "Prix Poly 1873 pour l'Excellence en Recherche" presented by the Ecole Polytechnique de Montreal on the occasion of its 125th anniversary, and the Urgel-Archambault Prize (the highest honor) in the field of physical sciences, mathematics and engineering from the French–Canadian Association for the Advancement of Science (ACFAS).